AD-A168 097 DAMAGE ASSESSMENT BY ACOUSTO-ULTRASONIC TECHNIQUES IN COMPOSITES(U) WASHINGTON UNIV ST LOUIS MO CENTER FOR COMPOSITES RESEARCH L LORENZO ET AL. APR 86 1/1

UNCLASSIFIED WU/CCR-86/2 N00014-85-K-0795 F/G 11/7 NL

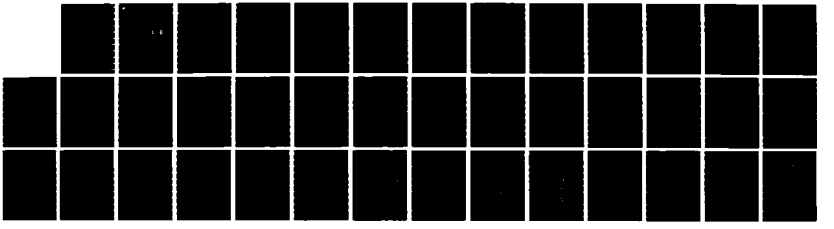

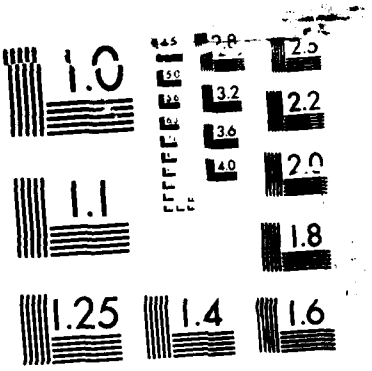

MICROCOPY RESOLUTION TEST CHART

WASHINGTON UNIVERSITY IN ST. LOUIS

CENTER FOR COMPOSITES RESEARCH

Report No. WU/CCR-86/2

AD-A168 097

DAMAGE ASSESSMENT BY ACOUSTO-ULTRASONIC TECHNIQUE IN COMPOSITES

Luis Lorenzo
H. Thomas Hahn

April 1986

Prepared for

Office of Naval Research
Arlington, VA 22217

WASHINGTON UNIVERSITY
CAMPUS BOX 1087
ST. LOUIS, MO 63130

Report WU/CCR-86/2

DAMAGE ASSESSMENT BY ACOUSTO-ULTRASONIC TECHNIQUE IN COMPOSITES

Luis Lorenzo
H. Thomas Hahn

Center for Composites Research
Washington University
St. Louis, MO 63130

April 1986

Supported by the Office of
Naval Research through
Grant No. N00014-85-K-0795

DAMAGE ASSESSMENT BY ACOUSTO-ULTRASONIC TECHNIQUE IN COMPOSITES

Luis Lorenzo and H. Thomas Hahn

Center for Composites Research

Washington University

St. Louis, Missouri 63130

ABSTRACT: This paper addresses the non-destructive evaluation of cross-ply $[0/90]_{2S}$ and $[90/0]_{2S}$ S-2 Gl/DER 332 laminates using acousto-ultrasonic and acoustic emission techniques. Acoustic emission and acousto-ultrasonic measurements gave early warnings of damage initiation before transverse cracks became visible. AU parameters such as peak amplitude, energy and stress wave factor were equally sensitive to damage initiation but peak amplitude and energy were more sensitive to damage accumulation. Variations of peak amplitude, event duration, ringdown counts, and rise time in AU tests were analyzed to show that internal damage not only increased the apparent attenuation but also affected the wave envelope. The same effect was also present in AE tests. Acousto-ultrasonic tests of an undamaged cross-ply laminate showed that the apparent attenuation coefficients were almost independent of the wave propagation direction. The strongest wave was found along the fibers in the ply in contact with the transducers and the weakest wave traveled at an angle of 45° to the fibers.

KEYWORDS: composite materials, glass/epoxy, cross-ply laminates, acoustic emission, acousto-ultrasonic technique, damage monitoring, ply cracking, attenuation, wave propagation.

INTRODUCTION

Acousto-Ultrasonic (AU) inspection is based on the interaction of an externally input stress wave with the internal structure of the material during its propagation to a receiving transducer. Obstacles to the wave front induce wave scattering, thereby increasing the apparent attenuation of the wave. Thus, wave characteristics can be correlated with material morphology, defects and internal damage present along the wave path.

Schultz [1] and Hastings et al. [2] placed transducers on the same face and measured the velocities of the transmitted waves. Egle and Brown [3] applied the same method to aluminum bars and plates for studying the effect of source location on the parameters of the transmitted wave but did not refer to AU as it is known presently. Not until the work of Vary and Bowles [4, 5], Vary and Lark [6] and Vary et al. [7] at NASA Langley Research Center in the late 70's did AU start to emerge as an independent NDE technique.

Vary and coauthors used AU as a novel inspection method by obtaining correlations between different material properties and wave parameters. With just a few exceptions, AU monitoring has been applied mainly to composite materials. The stress wave factor (SWF) was used as a prime measure of the internal efficiency of the material to transmit a stress wave [4-6]. SWF measurements were used as a method of characterizing the strength of 12-ply unidirectional AS/PMR-15 graphite/polyimide composites. The SWF correlated well with the interlaminar shear strength which was changed by using different cure pressures. Also, the SWF clearly indicated impact-damage in unidirectional AS/3501-6 [8].

Another important application of the SWF was in predicting the location

of fracture in composite specimens. Although the SWF attained minimum values in the expected failure locations in AS/PR-288 graphite/epoxy laminates of different stacking sequences [6], the exact correlation in E-glass/epoxy laminates depended to a large extent on the selection of proper parameters for conditioning and analyzing the transmitted waves [9].

Many researchers used the SWF in the past several years. However, it is not always this parameter that performs the best. Williams and Lampert [8] defined a modified stress wave factor as the ratio of the sum of the positive amplitudes of all oscillations exceeding a fixed threshold to an arbitrary reference voltage. The authors suggested that the modified SWF had better sensitivity than the original SWF. On the other hand, Lorenzo and Hahn [10] have shown that the peak amplitude and energy measured by commercial AE equipment gave better correlations than the original SWF.

The present paper presents results on damage assessment in composite laminates by acoustic emission (AE) and acousto-ultrasonic techniques. In particular, cross-ply S-2 glass/epoxy laminates are examined for correlation of AE parameters with damage accumulation. The main emphasis is on the detection of damage initiation and multiplication and the effect of damage and stacking sequence on apparent attenuation and wave envelope.

EXPERIMENTAL PROCEDURE

Materials

The composite laminates used were symmetric cross-ply S-2 glass/epoxy panels filament-wound at the Lawrence Livermore National Laboratory. The epoxy was DER 332/Methane Diamine (100/24.5) cured for 2 hours at 150°C. Two stacking sequences were studied: $[0/90]_{2S}$ and $[90/0]_{2S}$. Fiber volume

content varied between 65 and 67 % for different panels. Mechanical and hygrothermal properties of S-2 glass/DER 332 were reported in References [11] and [12].

Specimens

Specimen geometry is shown in Fig. 1. Principal dimensions and tabbing materials are listed in Table 1.

A 240 x 240 x 2 mm plate was used to measure apparent attenuation coefficients in AU mode in different directions of wave propagation.

Test Methods

Instrumentation and testing procedure have been described in Reference [10]. Parameters set up for AE and AU tests are indicated in Table 2.

In all AE and AU tests an AET AC375L resonant transducer was used as the receiving sensor. This transducer has a resonant frequency of 375 kHz with sensitivity better than -70 dB referred to 1 V/μbar. The emitting transducer in all AU tests was an AET FC500 broad-band transducer which has an almost flat frequency response between 200 kHz and 2.10 MHz with sensitivity better than -85 dB referred to 1 V/μbar. The attenuation was measured using an AET MAC425L resonant transducer as the receiver. Its resonant frequency is 425 kHz with a sensitivity better than -79 dB referred to 1V/μbar. Excitation in AU tests was by an AET Model 3001 pulser connected to a 5 V DC source.

For apparent attenuation measurements in the undamaged laminate an AEA AES-1L acoustic emission simulator was used to drive the emitting transducer. Input amplitude was 85 dB with rise and decay rates of 500 dB/msec. The carrier frequency was adjusted to be 430 kHz for maximum

reception. The plate was supported on a cellular rubber pad over a table. The emitting transducer was mounted at the center of the plate with silicone grease and a constant contact pressure of 0.160 MPa. The receiving transducer was positioned at distances of 45, 70 and 95 mm from the emitter forming different angles with the fiber orientation in the outer ply of the plate (Fig. 2). Silicone grease was also used maintaining a constant contact pressure of 0.072 MPa. For each orientation, three measurements were taken at each location. After each run, the receiving transducer was removed and cleaned. Grease was reapplied and the sensor was mounted back on. A total of 23 events were recorded in each run. Thus, reported amplitudes are average values of the amplitudes of 69 events. The only exception was the 67.5° orientation for which a total of six runs were taken, increasing the number of events to 138.

RESULTS AND DISCUSSION

Failure Process

Tensile properties and failure behavior of the specimens were reported in Reference [10] and will only briefly be summarized here for completeness.

In $[0/90]_{2S}$ specimens, cracks appeared first in the inner 90-degree plies and, later, in the outer 90-degree plies (Fig. 3). Cracks accumulated at a decreasing rate with increasing load with the crack density leveling off at high stresses.

In $[90/0]_{2S}$ specimens, cracks appeared first in the outer 90-degree plies (Fig. 4). Again, cracks accumulated at a decreasing rate. The outer 90-degree plies showed a similar behavior to the inner 90-degree plies in $[0/90]_{2S}$ specimens.

When cracking occurred audible noise was heard. Upon further loading, short, burst emissions accompanied slight drops in strain for both laminates.

After transverse cracks had developed, a large number of small inclined cracks appeared in the inner 90-degree plies of the $[0/90]_{2S}$ specimen and in the outer 90-degree plies of the $[90/0]_{2S}$ specimen. The same type of cracks were also observed to a lesser extent in the inner 90-degree plies of the $[90/0]_{2S}$ specimen. Inclined cracks originated at the interface between the 0- and 90-degree plies and grew towards a transverse crack. In $[90/0]_{2S}$ specimens, inclined cracks in the outer 90-degree plies grew without reaching the boundary surface. Also, in the outer plies of these specimens small transverse cracks originated at the outer surface and grew inward without reaching the interface between the 0- and 90-degree plies.

Delamination between the 0- and 90-degree plies was observed in specimens loaded up to 90 percent of the failure stress. In both laminates it was initiated and localized at the tips of transverse cracks in the inner 90-degree plies.

At applied stresses about 25 percent below the ultimate strength, groups of fibers in the outer 0-degree plies of $[0/90]_{2S}$ specimens failed and came loose at the edges. The resulting delamination progressively advanced towards the grips. This was not observed in $[90/0]_{2S}$ specimens. In the latter case, small groups of fibers from the inner 0-degree plies failed, and then came loose at stresses about 10 to 15 percent below the ultimate strength.

Epoxy was burnt off of a specimen loaded up to 90 percent of the failure stress and the specimen was examined on an optical microscope. No

fiber breaks were detected in any 0-degree ply.

Final failure was sudden with complete splitting of the 0-degree plies in both laminates.

Acoustic Emission

Figure 5 shows the total number of events as a function of applied stress. Emissions started earlier in the $[90/0]_{2S}$ specimen. In both laminates, acoustic activity started before cracking of the 90-degree plies was detected on an optical microscope or manifested itself as a knee-point in the stress-strain curves.

The rate of emission is initially slightly higher in the $[90/0]_{2S}$ specimen (Region I). Also, for a given stress the total number of events is greater, indicating a higher rate of accumulation of transverse cracks in the 90-degree plies of the $[90/0]_{2S}$ specimen.

In the $[0/90]_{2S}$ specimen, the cumulative event curve in Region III shows a discontinuity in slope at point B. This point corresponds to an instantaneous rate of emission equal to 357 events/s. At such a high rate, the equipment was saturated, and consequently, events were lost by the processor. The dashed line in Region III of Fig. 5 indicates an estimated emission output of the $[0/90]_{2S}$ specimen including lost events, assuming that the proportion of rejected events is the same as in the initial part of the curve. At point B, the average rate of emission decreased from 110.50 events/s (curve A-B) to 49.50 events/s (curve B-C). On the other hand, no events were lost for the $[90/0]_{2S}$ specimen, and the average event rate in Region III amounted to only 4.70 events/s (curve A-C').

Emissions detected in Region I are mainly the result of the cracking of 90-degree plies with instantaneous event rates as high as 170 events/s.

Thereafter, event rates decrease as a result of the decrease in the rate of crack accumulation. The high event rates in Region III of the $[0/90]_{2S}$ specimen is mainly due to the failure of the 0-degree plies at the edges and the initiation of delamination. The lack of such increased emissions in the $[90/0]_{2S}$ specimen is due partially to the increased attenuation associated with ply cracks. The highly cracked outer 90-degree ply is unable to transmit the waves generated within the specimen. Cracks act in this case as a source of attenuation. In the $[0/90]_{2S}$ specimen, however, the 0-degree ply is in contact with the transducer. Thus, elastic waves generated within or underneath this ply can travel to the receiving sensor using the fibers as wave guides [13, 14].

The hypothesis that events from 0-degree ply failure were not detected in the $[90/0]_{2S}$ specimen was also confirmed by mean peak amplitude and mean event duration outputs, Figs. 6 and 7. Mean values were obtained as averages over a 10 second interval. In the $[0/90]_{2S}$ specimen, events in Region III have higher peak amplitudes and longer durations than those in Regions I and II, indicating more energetic failures in Region III. However, in the $[90/0]_{2S}$ specimen, events in Region III are less energetic than those in Regions I and II. The higher peak amplitudes and longer event durations in Region I of the $[90/0]_{2S}$ specimen are likely to be due to the better wave transmission in the outer ply, which is in contact with the transducer, at early stages of cracking. In the $[0/90]_{2S}$ specimen, elastic waves generated in the 90-degree plies have to face one or more interfaces before reaching the outer ply. At each interface, reflection and refraction occur with mode changes [15, 16]. Thus, the energy content of the refracted wave in the outer ply is likely to be lower in the $[0/90]_{2S}$ specimen.

In both types of laminates, events in Region I have higher amplitudes and longer durations at stresses between 100 and 150 MPa. This stress range corresponds to the appearance of ply cracks and their accumulation at the highest rates, Figs. 3 and 4. As the rate of crack accumulation decreases in Region II, mean parameters fluctuate in the $[0/90]_{2S}$ specimen. On the other hand, in the $[90/0]_{2S}$ specimen peak amplitude and event duration in Region II decrease sharply; thereafter, they start to fluctuate. In the $[0/90]_{2S}$ specimen, peak amplitude and event duration initially increase in Region III (curve A-B). When saturation occurs, however, they decrease slightly. In Regions II and III, events in the $[0/90]_{2S}$ specimen show higher peak amplitudes and longer durations than those in the $[90/0]_{2S}$ specimen. At this stage of loading, cracks are fully developed and attenuate waves more effectively in the $[90/0]_{2S}$ specimen.

Figures 8 and 9 show cumulative and density distributions of amplitude and event duration, respectively. Events lost in the $[0/90]_{2S}$ specimen are not included in these figures. At low amplitudes, both specimens show approximately the same cumulative distribution. However, the $[0/90]_{2S}$ specimen shows a greater proportion of high-amplitude events than does the $[90/0]_{2S}$ specimen. Also, the proportion of long-duration events is greater in the $[0/90]_{2S}$ specimen. It is noted that low amplitude and short duration are characteristic of events from ply cracks while high-amplitude, long-duration events correspond to a more energetic failure mode such as fiber breaks and delamination at high strain levels [13, 17, 18].

The large number of events with amplitude 63 dB in Fig. 8 is an artifact of the equipment limitation. Since the maximum recordable amplitude is 63 dB, emissions with amplitudes equal to or higher than 63 dB

are assigned an amplitude of 63 dB. Thus, it is not possible to analyze the behavior at higher amplitudes since the upper tail end of the distributions are not known.

Acousto-Ultrasonic Tests

Three parameters were considered for AU correlation: amplitude, energy and stress wave factor (SWF). Those parameters were normalized with respect to their respective values in the undamaged state.

The amplitude ratio V/V_o is defined as the ratio of the peak amplitude of the wave after a given loading to that in the undamaged initial state. This ratio is related to the amplitudes I and I_o expressed in dB by

$$V/V_o = 10^{[(I - I_o)/20]} \tag{1}$$

The energy ratio E/E_o is defined similarly noting that the energy is proportional to the area under the voltage squared versus time curve. Thus, assuming a bilinear envelope for the voltage-time curve, the ratio is obtained as

$$E/E_o = (V/V_o)^2 \ (T/T_o) \tag{2}$$

where T and T_o are the event durations. Note that in this case two AE parameters are involved.

SWF is obtained by relating ringdown counts, pulse repetition rate and reset time as defined in Reference [4]. Since the pulse repetition rate and the reset time were constant in all tests, the stress wave factor ratio SWF/SWF_o is equal to the ratio of ringdown counts between the undamaged and damaged states.

within the specimen while the rise time is the most unpredictable. Note that no clear correlation seems to exist between the changes of peak amplitude, ringdown counts and event duration [13].

One possible explanation for the absence of apparent correlation is the effect that defects have on a traveling wave. When defects such as cracks exist along the wave path, wave scattering occurs at cracks. Thus, when the wave train passes through cracks its envelope changes.

The change of wave envelope due to damage may appear not only in AU testing but also during AE monitoring. Mean peak amplitudes and mean event durations of events over a one-second interval from AE tests were analyzed to see if internal damage affected AE results. Figure 15 shows the change of amplitude-to-duration ratio with stress in the $[90/0]_{2S}$ specimen. Initially, the ratio decreases indicating a slight broadening of wave envelope. However, when many cracks develop above 200 MPa, no trend can be detected in the change of wave envelope. Emissions in the $[0/90]_{2S}$ specimen are more consistent regardless of the stress level. The average wave envelope becomes slightly steeper as the stress increases, Fig. 16. One of the reasons for less variation in the $[0/90]_{2S}$ specimen is again the lower apparent attenuation, which decreases the scatter in amplitude [22].

Attenuation

The dependence of attenuation on material properties, wave frequency and applied stress has been well characterized [23-31]. However, the effect of internal damage on attenuation in laminated composites has received little attention. Results discussed so far show that the apparent attenuation depends on stacking sequence and internal damage. For each stacking sequence, the apparent attenuation increased from a minimum in the

undamaged state to a maximum near failure. The additional attenuation was due to the wave scattering by transverse cracks in the 90-degree plies.

In order to gain an insight into the dependence of attenuation on stacking sequence without damage, a cross-ply laminate was tested in AU mode with different distances between transducers, Fig. 2.

Figure 17 shows the peak amplitudes changing with the fiber orientation angle in the external ply. The fiber orientation angle is 0 when the transducers are aligned parallel to the fibers. The highest amplitudes are seen at 0° and the lowest at 45°. For each transducer spacing, the amplitude curve is not symmetric with respect to the 45°-orientation, with amplitudes being higher when the orientation angle is less than 45°.

Figure 18 shows variations of peak amplitude with the transducer spacing in different propagation directions. The data were fitted with an exponentially decaying law of the form

$$V = V_o \exp(-2\alpha x) \tag{3}$$

where V is the peak amplitude when the transducer spacing is x. The calculated values of V_o and α are shown in Fig. 19. Note that the reference amplitude V_o is the value of V at the origin $x = 0$, and α is the coefficient of apparent attenuation.

The reference amplitude V_o shows a strong dependence on the direction of wave propagation similarly to the amplitude V. However, the apparent attenuation coefficient fluctuates between 0.005 and 0.01 neper/mm independent of the direction of propagation, Fig. 19. The mean value is 0.0078 neper/mm with a coefficient of variation of about 0.19. It is noted that in ultrasonic through-transmission tests attenuation coefficients

depend on the direction of wave propagation, for example, parallel or normal to the fibers [27, 30, 31]. However, no such dependence is observed in AU test results.

CONCLUSIONS

1. Both AE and AU techniques can be used to detect ply cracking. Event counts, peak amplitude, energy, and SWF are sensitive to ply cracking. Energy is the most sensitive AU parameter while peak amplitude shows the least variation from specimen to specimen.

2. Peak amplitude and energy are more sensitive to crack accumulation than SWF. As cracks develop, these parameters decrease substantially. Peak amplitude shows the least variation from specimen to specimen.

3. Apparent attenuation increases with internal damage and depends on the stacking sequence. Increased attenuation due to damage may hamper detection of emissions, as shown in the $[90/0]_{2S}$ specimen.

4. Wave scattering at internal cracks may change the wave envelope. As a result, event duration, ringdown counts and rise time can even increase as more cracks develop. However, peak amplitude decreases monotonically with increasing damage.

5. The modification of wave envelope also affects AE results. No correlation is observed between peak amplitude and event duration especially in the $[90/0]_{2S}$ specimen.

6. The intensity of the wave generated in AU tests depends on the direction of propagation; however, the apparent attenuation is almost independent of the propagation direction.

REFERENCES

1. Schultz, A. W.: "Development and Application of Nondestructive Methods for Predicting Mechanical Properties of Advanced Reinforced Nonmetallic Composites," Technical Report AFML-TR-71-168, Air Force Materials Laboratory, Dayton, Ohio, April 1971.

2. Hastings, C. H., E. F. Olster and S. A. Lopilato: "Development and Application of Nondestructive Methods for Predicting Mechanical Properties of Advanced Reinforced Nonmetallic Composites," Technical Report AFML-TR-73-157, Air Force Materials Laboratory, Dayton, Ohio, May 1973.

3. Egle, D. M. and A. E. Brown: "Considerations for the Detection of Acoustic Emission Waves in Thin Plates," Journal of the Acoustical Society of America, Vol. 57, No. 3, 1975, pp. 591-597.

4. Vary, A. and K. J. Bowles: "Ultrasonic Evaluation of the Strength of Unidirectional Graphite-Polyimide Composites," NASA Memorandum TMX-73646, National Aeronautics and Space Administration, Washington, D.C., 1977.

5. Vary, A. and K. J. Bowles: "Use of an Ultrasonic-Acoustic Techniques for Nondestructive Evaluation of Fiber Composite Strength," NASA Memorandum TM-73813, 1978.

6. Vary, A. and R. F. Lark: "Correlation of Fiber Composite Tensile Strength with the Ultrasonic Stress Wave Factor," Journal of Testing and Evaluation, JTEVA, Vol. 7, No. 4, 1979, pp. 185-191.

7. Vary, A., P. E. Moorhead and D. R. Hull: "Metal Honeycomb to Porous Wireform Substrate Diffusion Bond Evaluation," Proceedings of the 1982 Spring ASNT Meeting, Boston, Mass., April, 1982.

8. Williams, J. H., Jr. and N. R. Lampert: "Ultrasonic Nondestructive Evaluation of Impact-Damaged Graphite Fiber Composite," NASA Report CR 3293, National Aeronautics and Space Administration, Washington, D.C., 1980.

9. Vary, A. in Mechanics of Nondestructive Testing, W. W. Stinchcomb, Ed., Plenum Pub. Co., New York, 1980, pp. 123-141.

10. Lorenzo, L. and H. T. Hahn: "Detection of Ply Cracking through Wave Attenuation," Proceedings of the 29th National SAMPE Symposium, 1984, pp. 1022-1033.

11. Hahn, H. T., D. G. Hwang, W. K. Chin and S. Y. Lo: "Mechanical Properties of a Filament-Wound S-2 Glass/Epoxy Composite for Flywheel Application," Lawrence Livermore National Laboratory, UCRL-15365, March 1982.

12. Lo, S. Y.: "Hygrothermal Expansion of Kevlar 49/Epoxy and S-2 Glass/Epoxy Composites," Master of Science Thesis, Department of Mechanical

Engineering, Washington University, December 1982.

13. Lorenzo, L. and H. T. Hahn: "Acoustic Emission Study of Fracture of Fibers Embedded in Epoxy Matrix," Proceedings of the First International Symposium on Acoustic Emission from Reinforced Composites, SPI, 1983, Session 2.

14. Ono, K. and R. De Spain: "Characterization of Carbon Fiber Composites Using Acousto-Ultrasonic Techniques," Proceedings of the First International Symposium on Acoustic Emission from Reinforced Composites, SPI, 1983, Session 6.

15. Ewig, W. M., W. Jardetzky and F. Press, Elastic Waves in Layered Media, McGraw Hill Book Co., New York, 1957.

16. Brekhovskikh, L. M., Waves in Layered Media, Academic Press, New York, 1980.

17. Hamstad, M. A.: "Acoustic Emission from Filamentary-Wound Pressure Bottles," Proceedings of the 4th SAMPE National Technical Conference, 1972, pp. 321-333.

18. Scarpellini, R. S.; T. L. Swanson and T. J. Fowler: "Acoustic Emission Signatures of RP Defects," Proceedings of the First International Symposium on Acoustic Emission from Reinforced Composites, SPI, 1983, Session 3.

19. Williams, J. H., Jr., H. Karagulle and S. S. Lee: "Ultrasonic Input-Output for Transmitting and Receiving Longitudinal Transducers Coupled to Same Face Isotropic Elastic Plate," NASA Report CR 3506, National Aeronautics and Space Administration, Washington, D.C., 1982.

20. Karagulle, H., J. H. Williams, Jr. and S. S. Lee: "Stress Waves in an Isotropic Elastic Plate Excited by a Circular Transducer," NASA Report CR 3877, National Aeronautics and Space Administration, Washington, D.C.,1985.

21. Williams, J. H., Jr., H. Karagulle and S. S. Lee: "Ultrasonic Testing of Plates Containing Edge Cracks," NASA Report CR 3904, National Aeronautics and Space Administration, Washington, D.C., 1985.

22. Lorenzo, L and H. T. Hahn: "On the Applicability of Amplitude Distribution Analysis to the Fracture Process of Composite Materials," to appear in Journal of Acoustic Emission.

23. Sve, C.: "Stress Wave Attenuation in Composite Materials," Journal of Applied Mechanics, Transactions, American Society of Mechanical Engineers, December 1972, pp. 1151-1153.

24. Sutherland, H. J. and R. Lingle: "Geometric Dispersion of Acoustic Waves by a Fibrous Composite," Journal of Composite Materials, Vol. 6, 1972, pp. 490-502.

25. Sutherland, H. J. and R. Lingle: "An Acoustic Characterization of Polymethyl Methacrylate and Three Epoxy Formulations," Journal of Applied Physics D, Vol. 43, 1972, pp. 4022-4026.

26. Tauchert, T. R. and N. N. Hsu: "Influence of Stress upon Internal Damping in a Fiber Reinforced Composite Material," Journal of Composite Materials, Vol. 7, 1973, pp. 516-520.

27. Tauchert, T. R.: "Internal Damping in a Fiber-Reinforced Composite Material," Journal of Composite Materials, Vol. 8, 1974, pp. 195-199.

28. Felix, M. P.: "Attenuation and Dispersion Characteristics of Various Plastics in the Frequency Range 1-10 MHz," Journal of Composite Materials, Vol. 8, 1974, pp. 275-287.

29. Sutherland, H. J.: "Dispersion of Acoustic Waves by Fiber-Reinforced Viscoelastic Materials," Journal of the Acoustical Society of America, Vol. 57, 1975, pp. 870-875.

30. Williams, J. H., Jr., H. N. Hashemi and S. S. Lee: "Ultrasonic Attenuation in AS/3501-6 Graphite/Epoxy Fiber Composite," NASA Report CR 3180, National Aeronautics and Space Administration, Washington, D.C., 1979.

31. Lee, S. S. and J. H. Williams, Jr.: "Stress Wave Attenuation in Thin Structures by Ultrasonic Through-Transmission," NASA Report CR 3203, National Aeronautics and Space Administration, Washington, D.C., 1980.

Table 1: Specimen Geometry

Test	GL mm	L mm	W mm	t mm	α deg	Tab Material
ASTM D-3039-76	129	220	12.70	2	10	Glass Fabric/Polyester
AE	170	240	25.00	2	90	Aluminum
AU	170	240	25.00	2	10	Glass Fabric/Polyester

Table 2: Preset Parameters for AE and AU Tests [10]

Parameter	AU	AE
Preamplifier Gain (dB)	60	60
Amplifier Gain (dB)	30	10
Threshold Voltage (V, Fixed)	1.00	1.50
Event Duration Clock (nsec)	125	125
Dead Time (μsec)	32	32
Rise Time Clock (nsec)	125	125
Pulse Rate (pulses/sec)	2.5	
Acceptance Criterion:		
- Ringdown Counts		$2 \leq n \leq 4095$
- Peak Amplitude (dB)		$29 \leq I \leq 64$
- Event Duration (μsec)		$2 \leq T \leq 480$
- Rise Time (μsec)		$2 \leq T_r \leq 480$

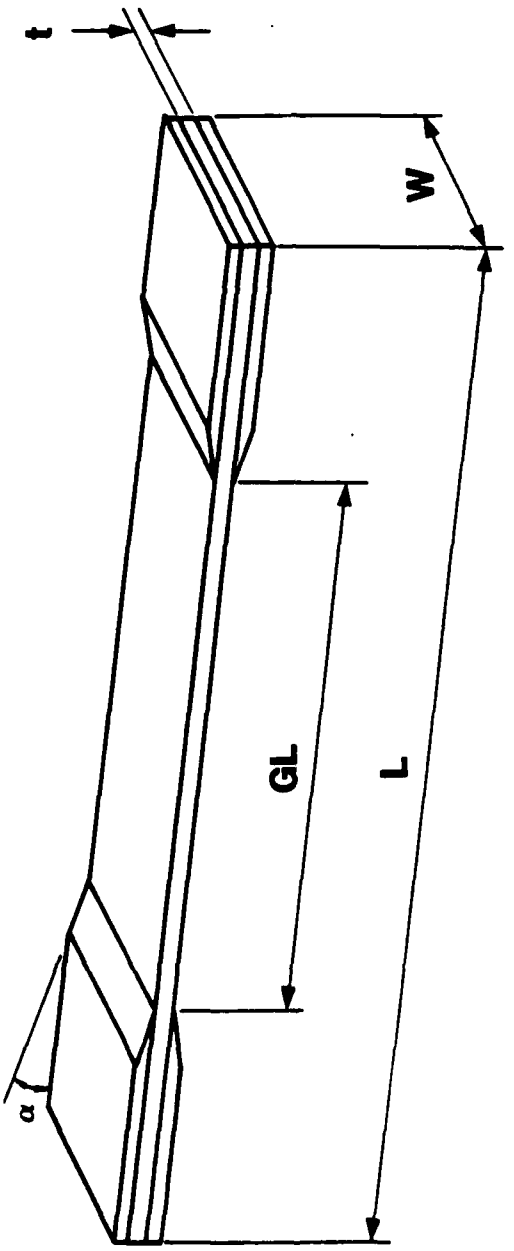

Figure 1. Specimen Geometry

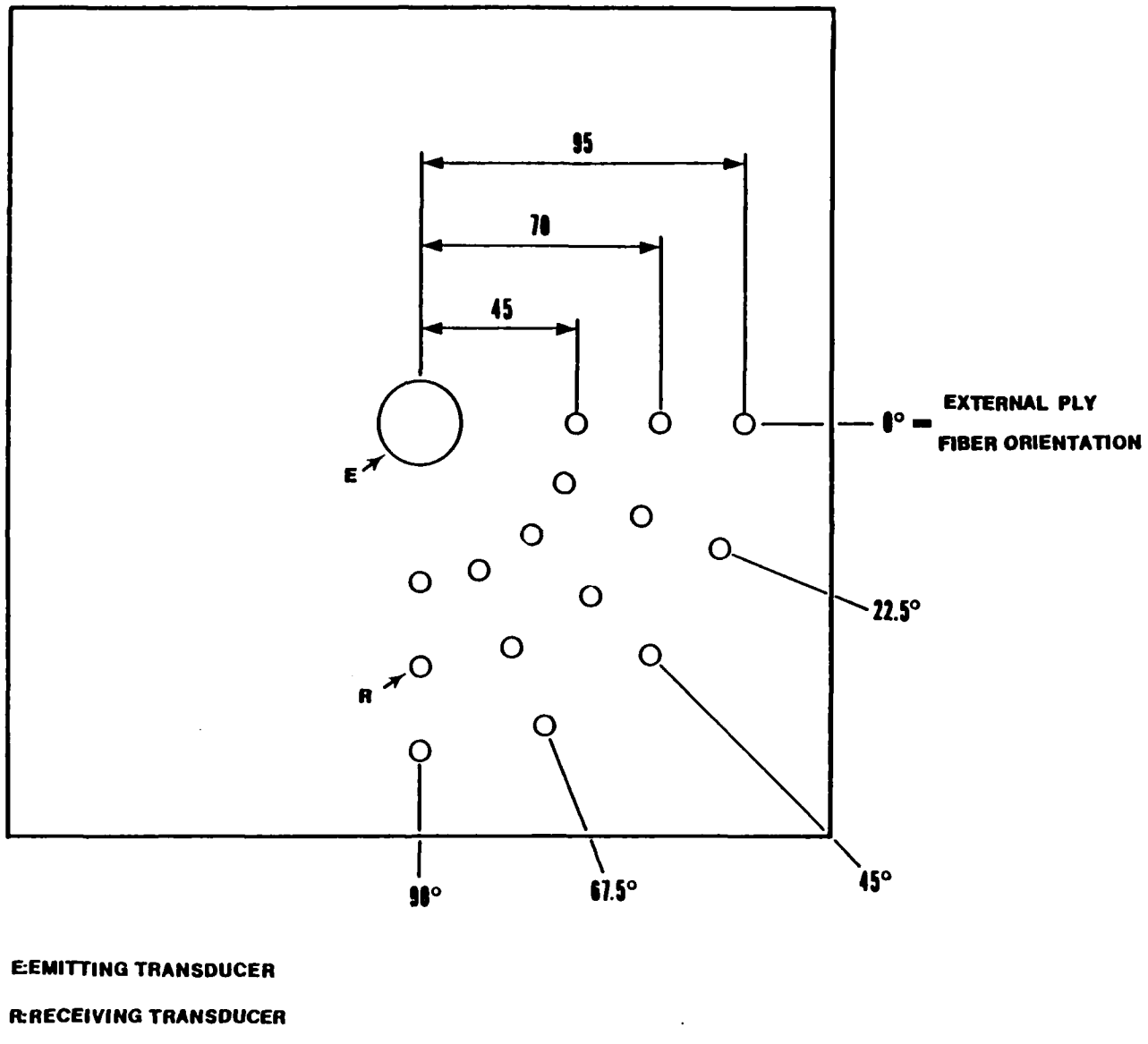

Figure 2. Plate Specimen for Attenuation Measurements

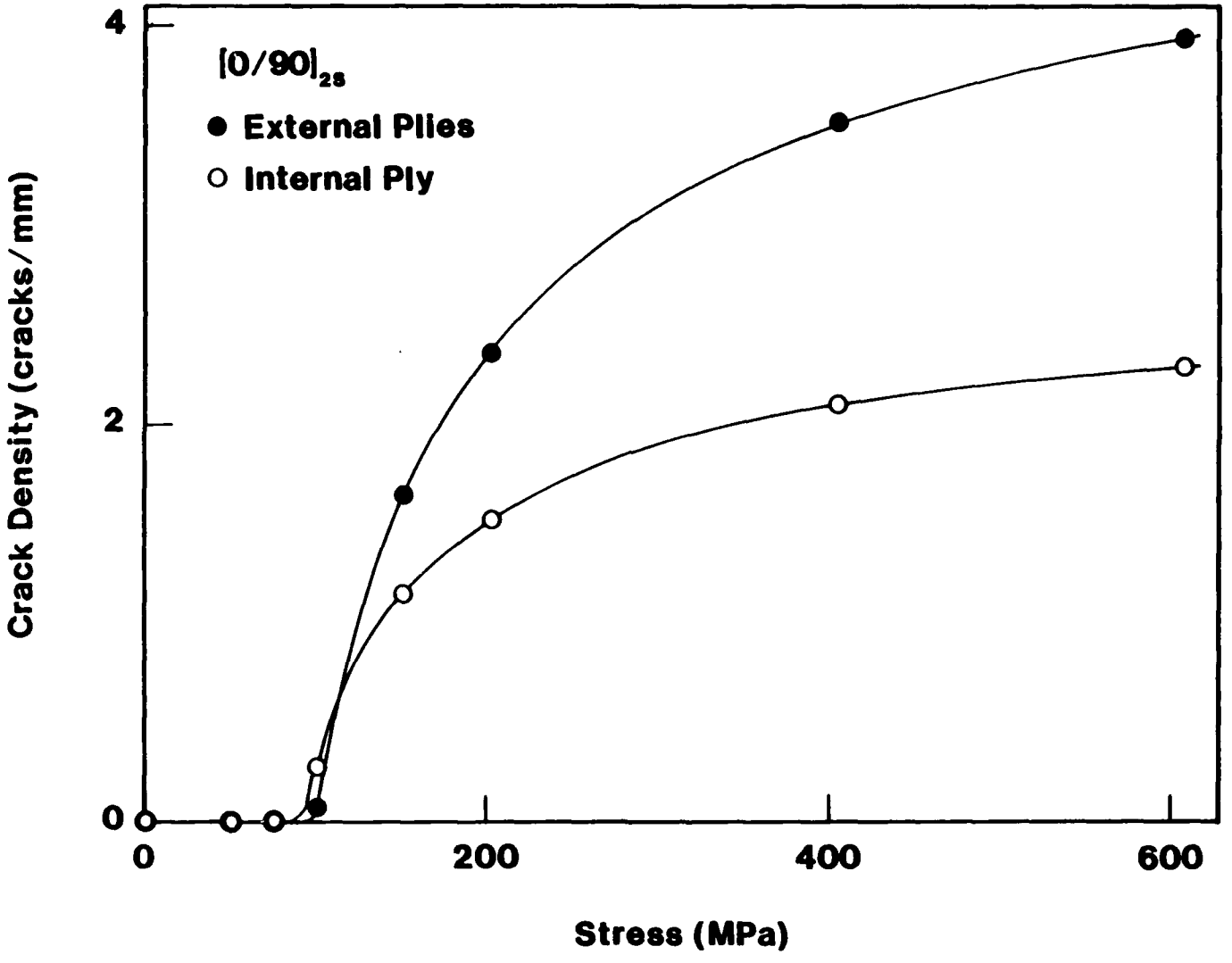

Figure 3. Crack Density Increasing with Stress in $[0/90]_{2S}$ Specimen [10]

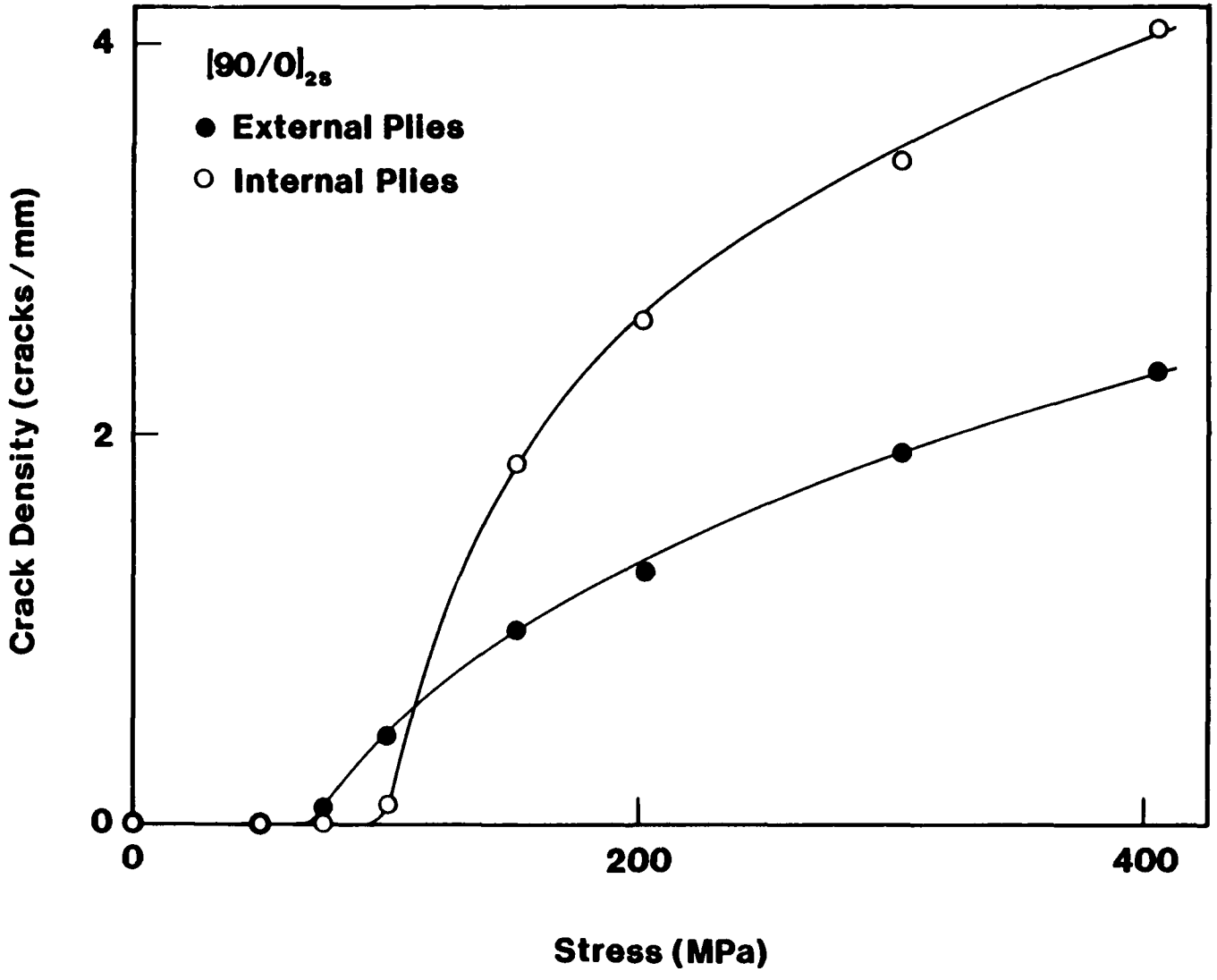

Figure 4. Crack Density Increasing with Stress in $[90/0]_{2S}$ Specimen [10]

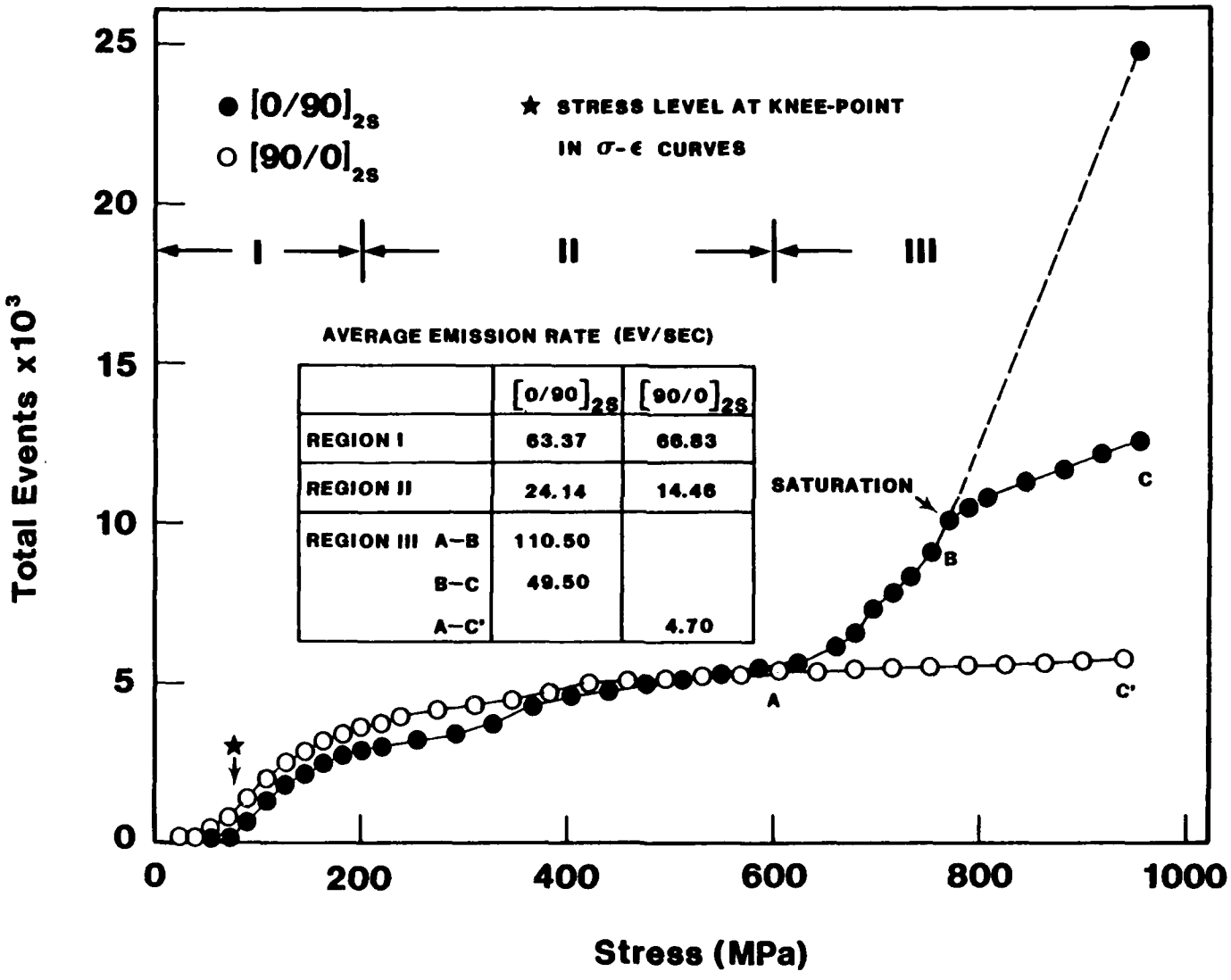

	[0/90]2S	[90/0]2S
REGION I	63.37	66.83
REGION II	24.14	14.46
REGION III A–B	110.50	
B–C	49.50	
A–C'		4.70

Figure 5. Cumulative Events

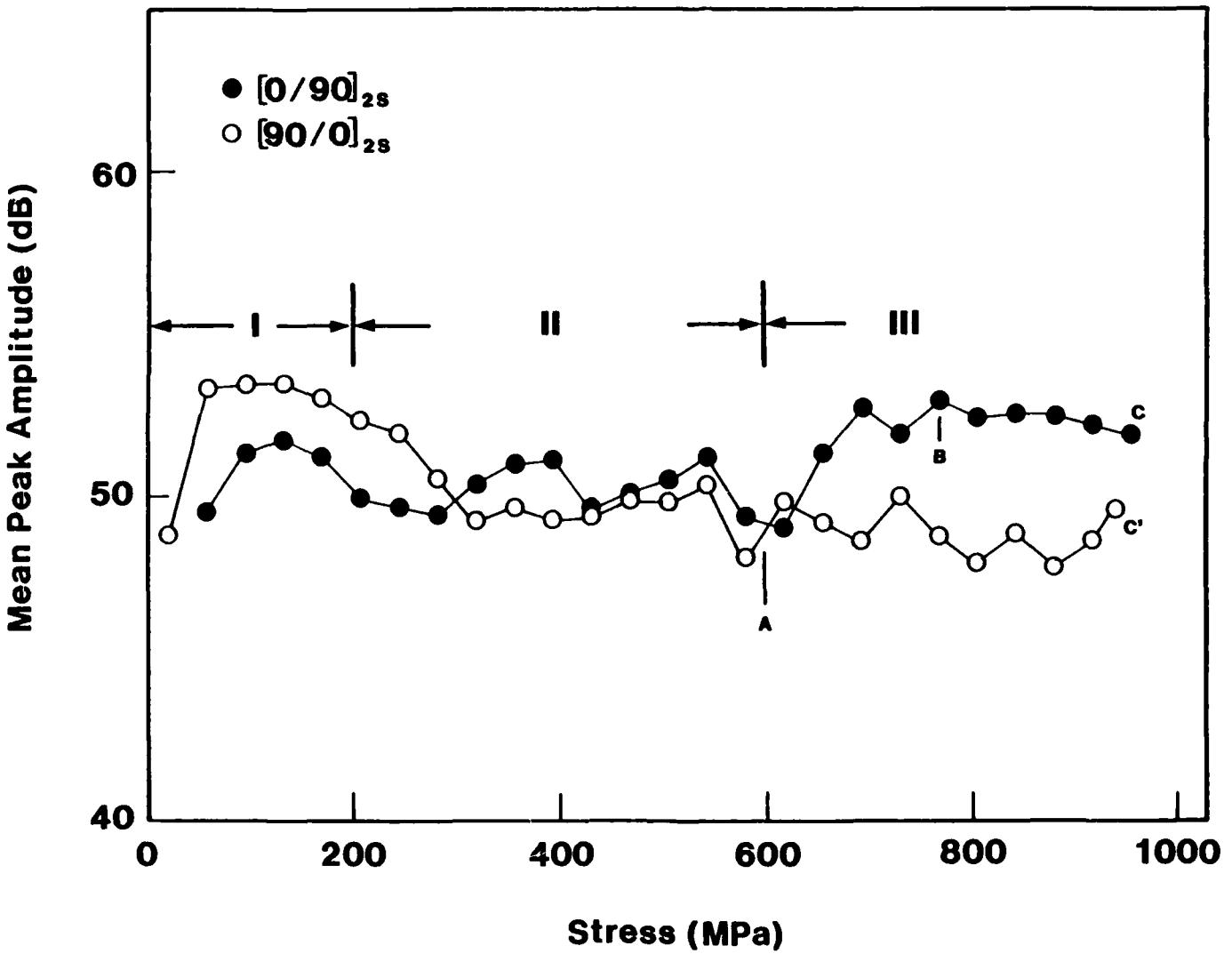

Figure 6. Mean Peak Amplitude as a Function of Stress (Mean values over a 10-second interval)

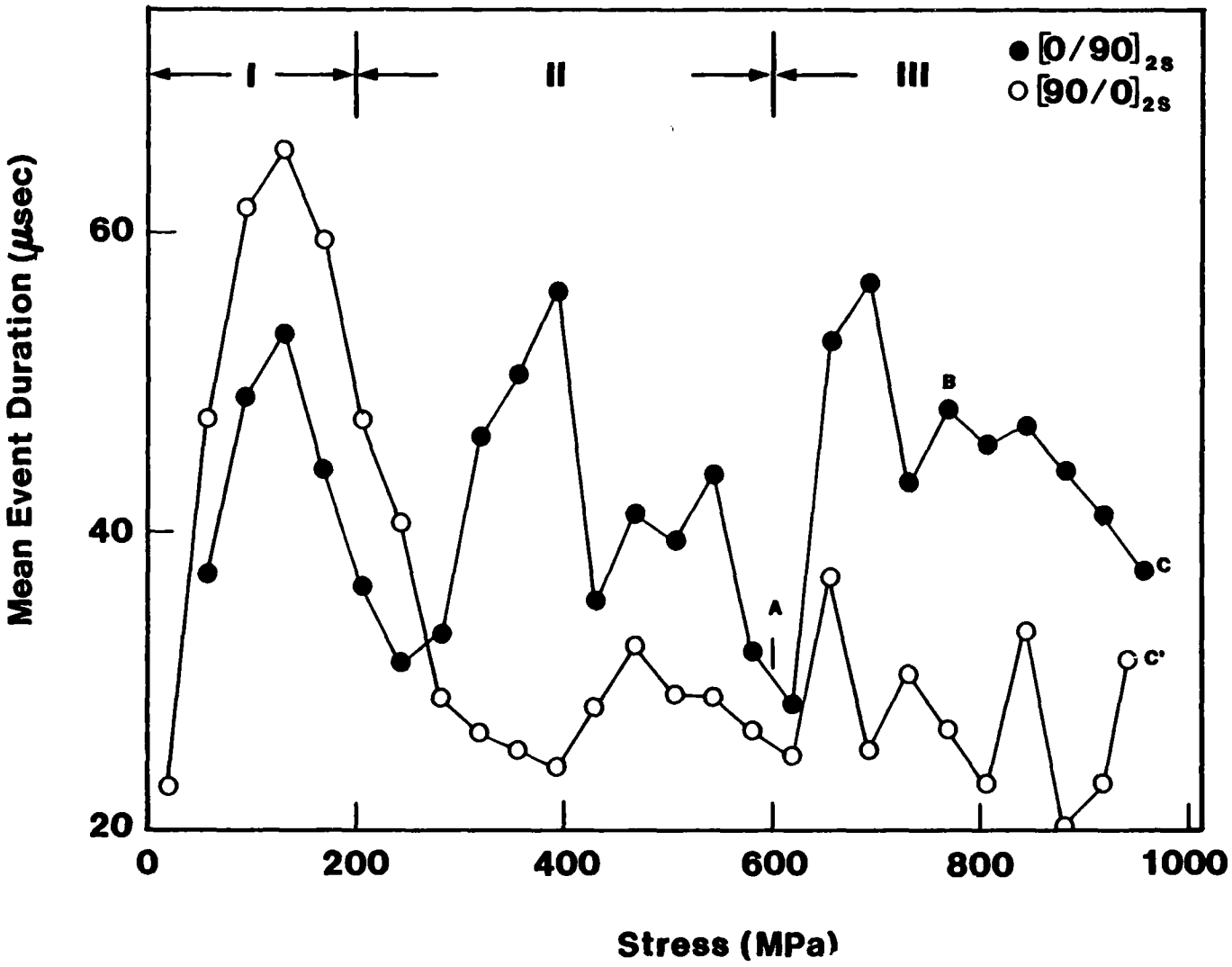

Figure 7. Mean Event Duration as a Function of Stress (Mean values over a 10-second interval)

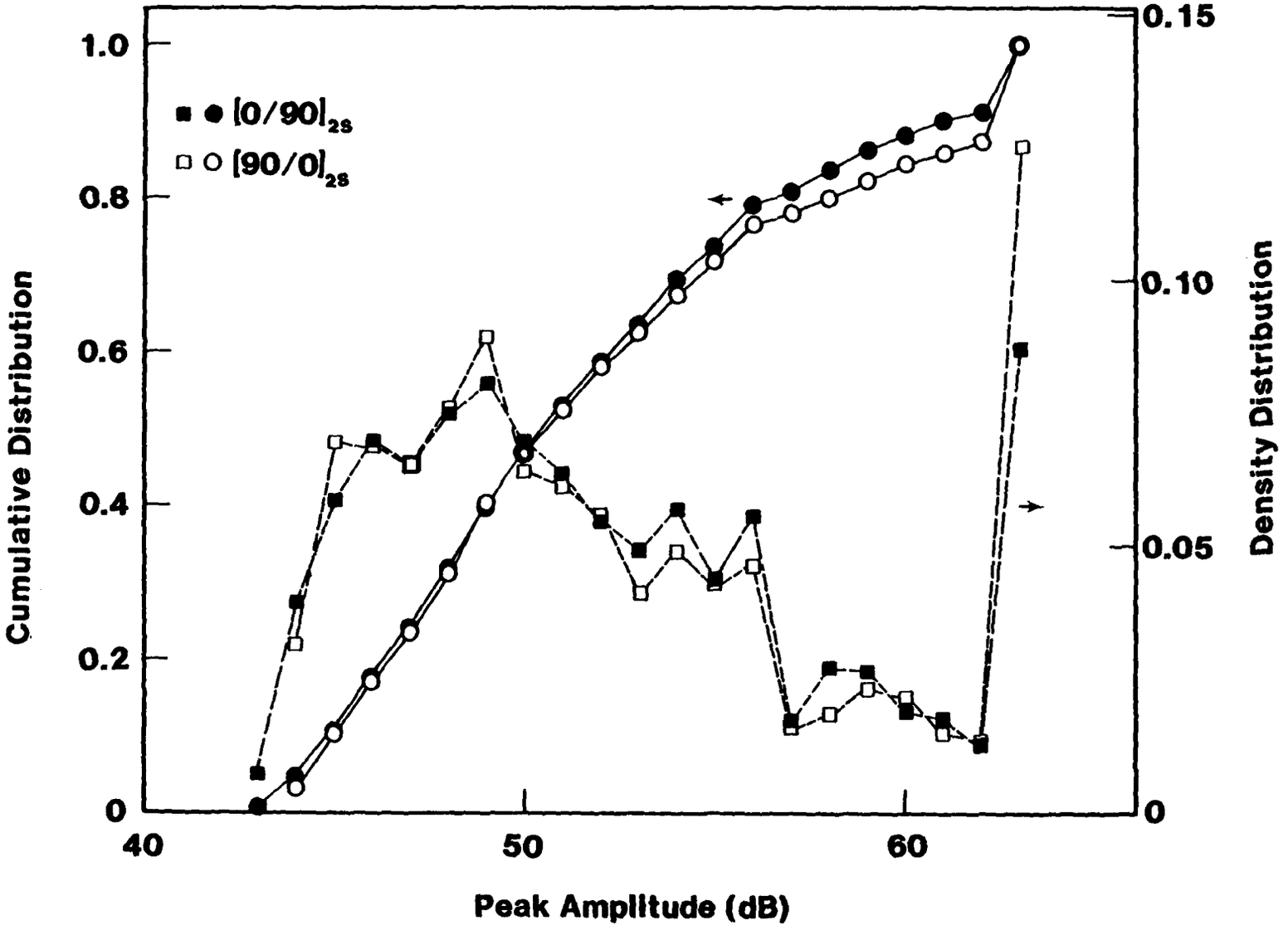

Figure 8. Cumulative and Density Distributions of Peak Amplitude

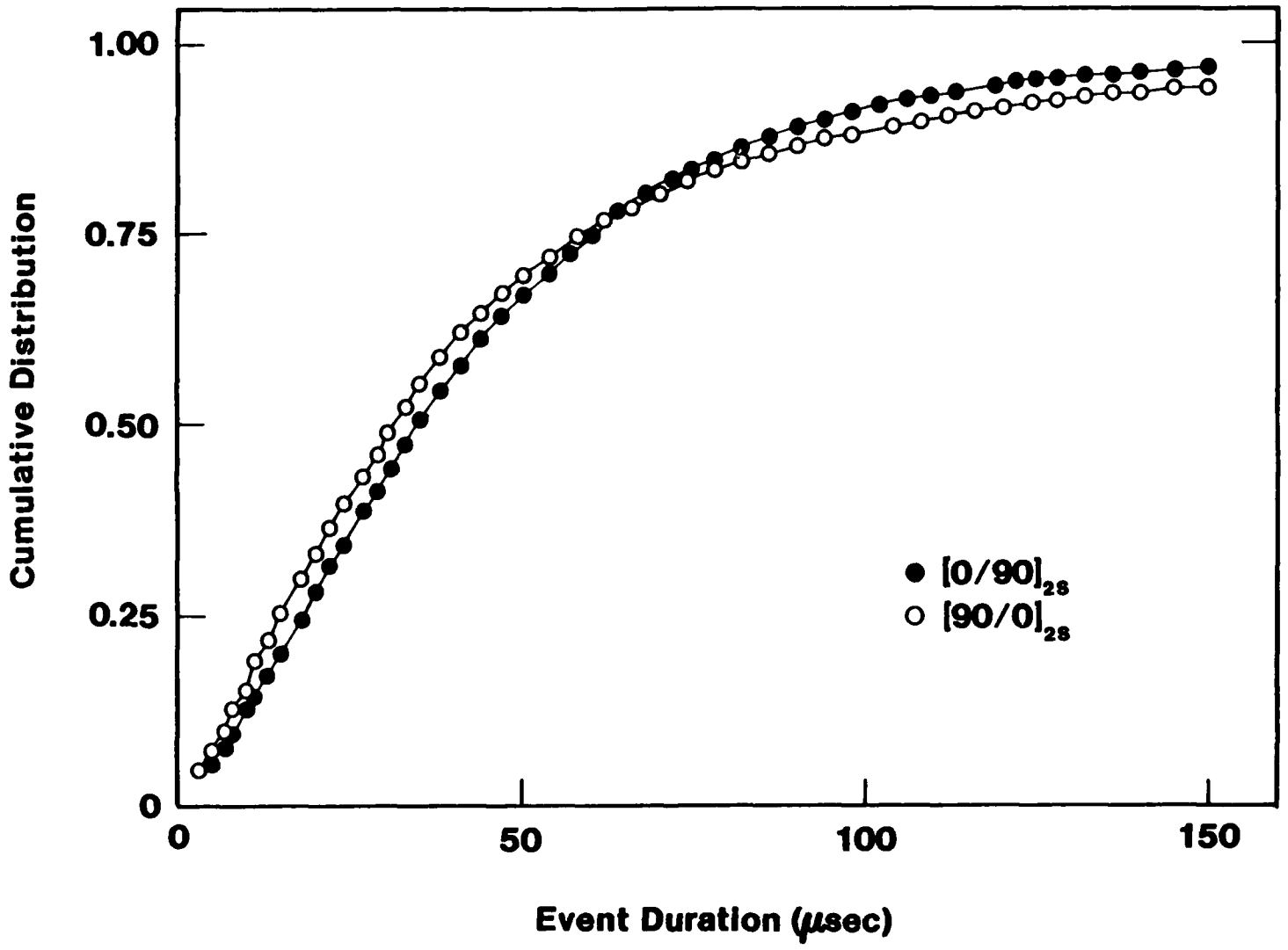

Figure 9. Cumulative Distribution of Event Duration

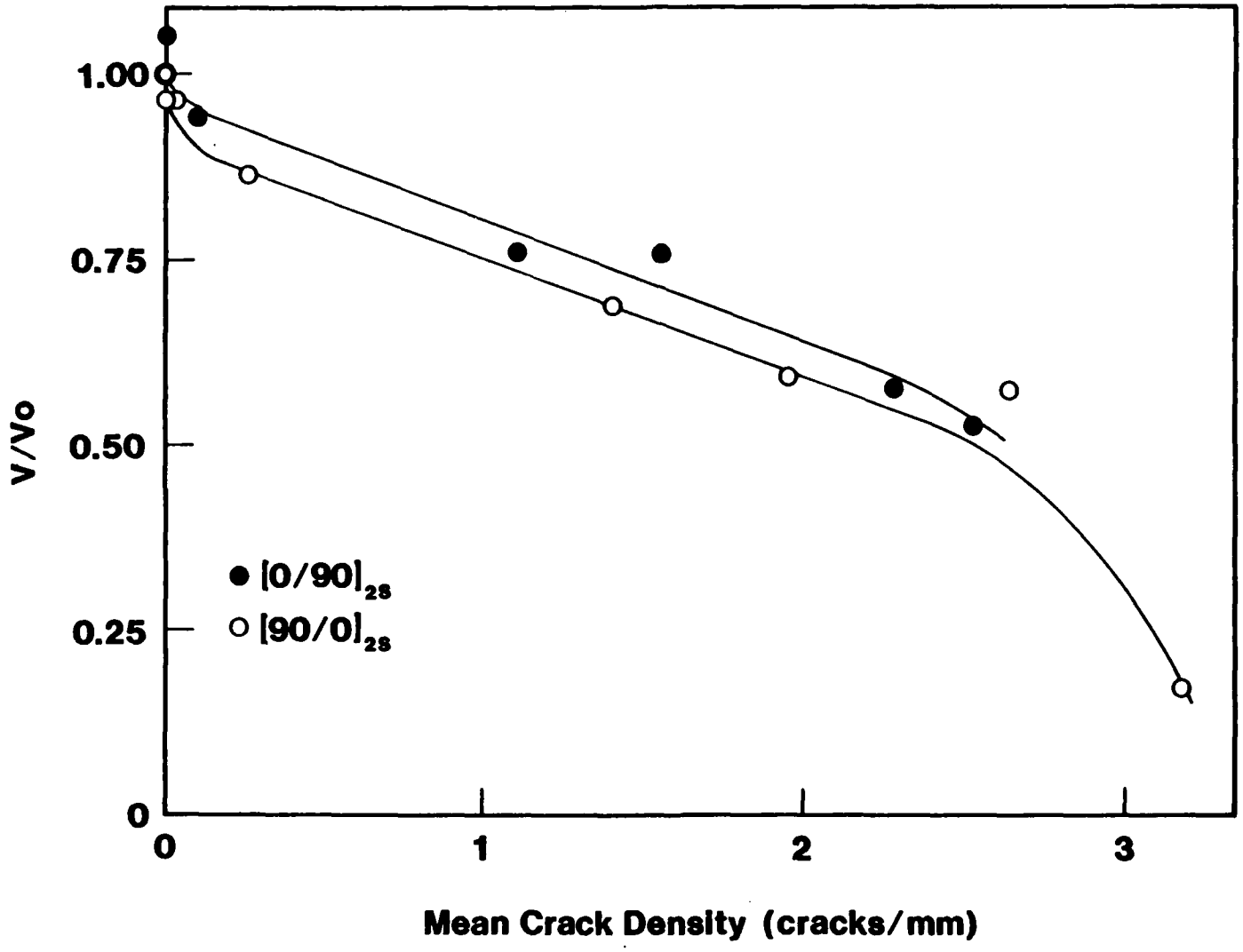

Figure 10. Dependence of Amplitude Ratio on Mean Crack Density [10]

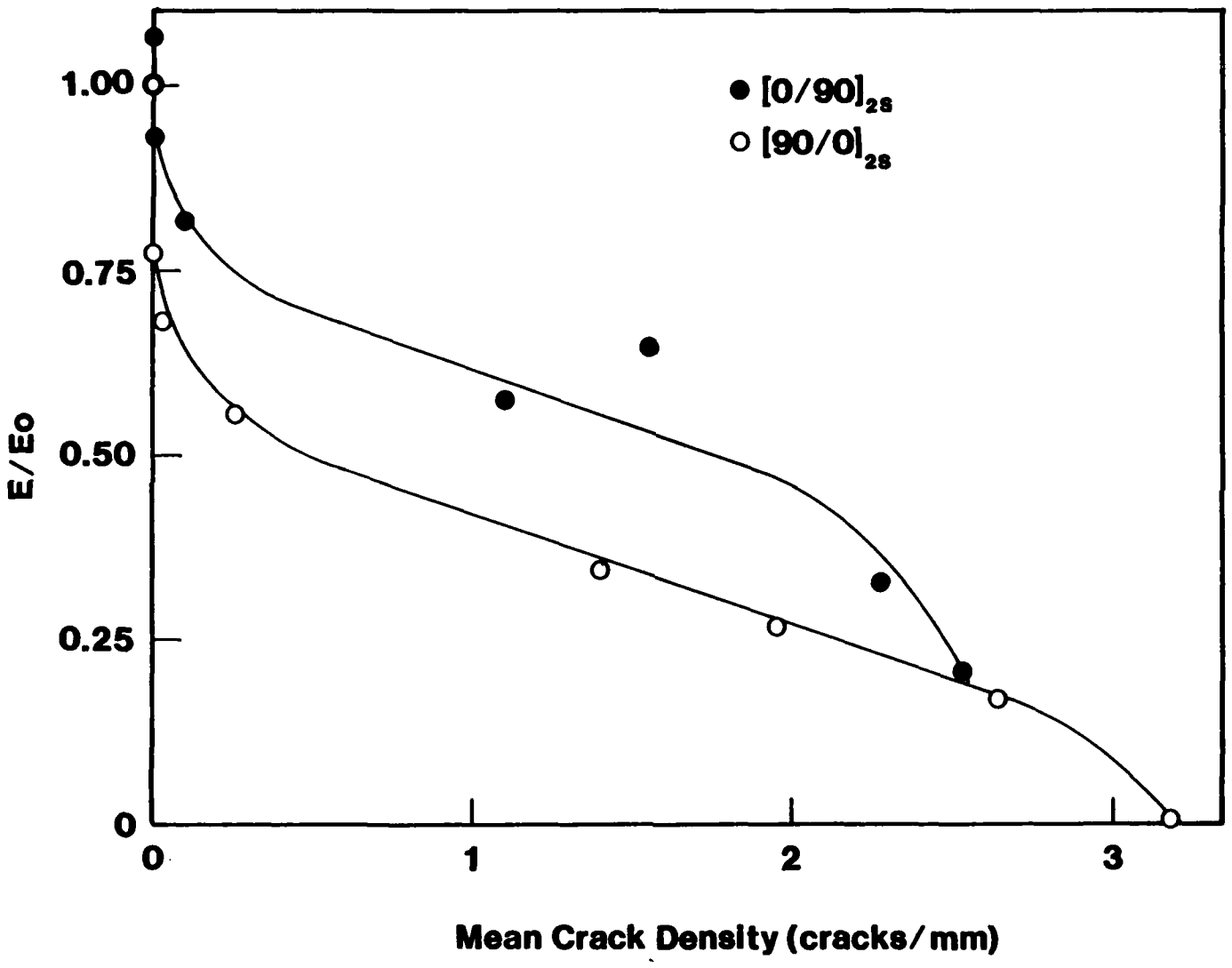

Figure 11. Dependence of Energy Ratio on Mean Crack Density [10]

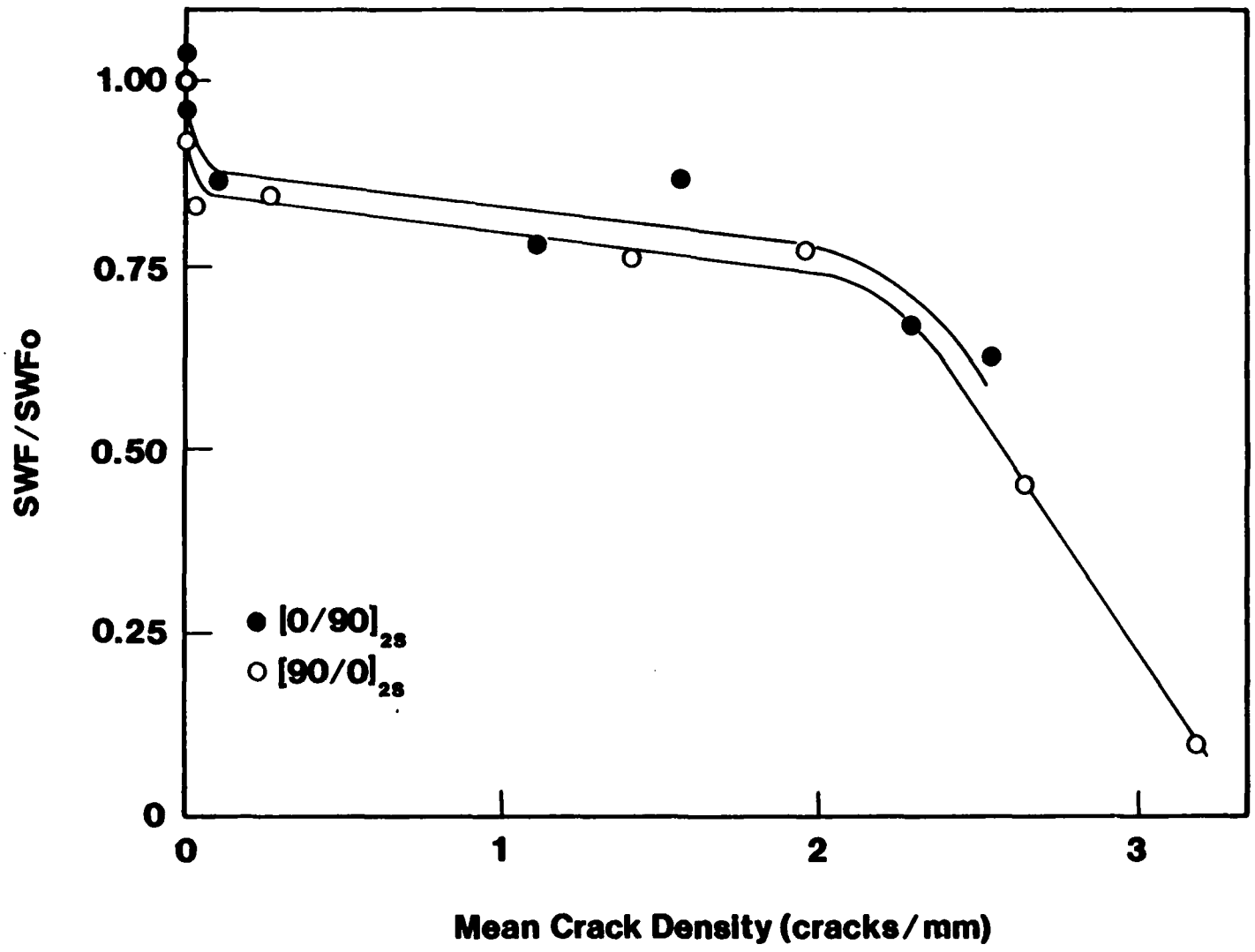

Figure 12. Dependence of Stress Wave Factor Ratio on Mean Crack Density

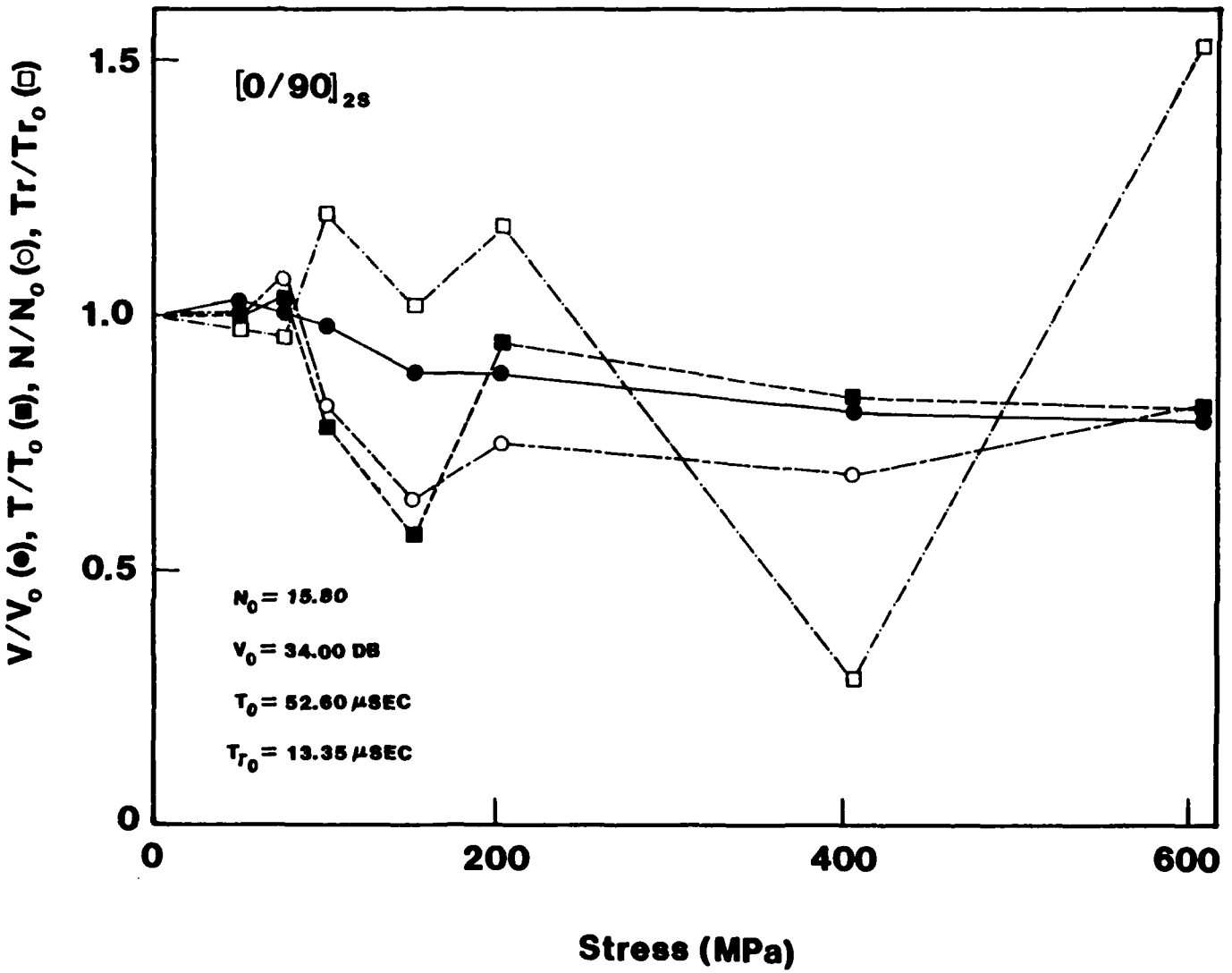

Figure 13. Peak Amplitude (V/V_o), Event Duration (T/T_o), Ringdown Counts (N/N_o) and Rise Time ($T_r/(T_r)_o$) Ratios versus Stress in $[0/90]_{2S}$ Specimen

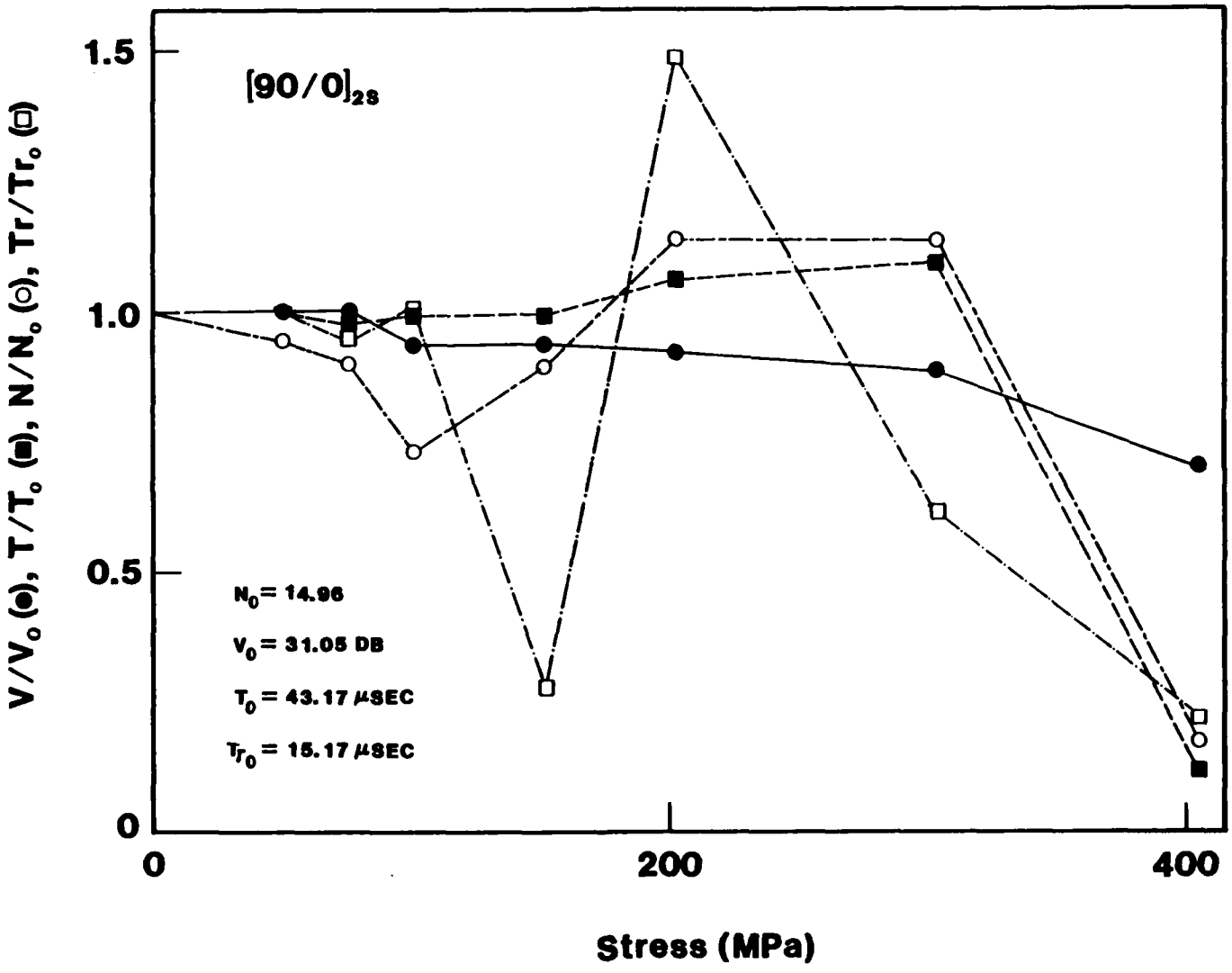

Figure 14. Peak Amplitude (V/V_o), Event Duration (T/T_o), Ringdown Counts (N/N_o) and Rise Time ($T_r/(T_r)_o$) Ratios versus Stress in $[90/0]_{2S}$ Specimen

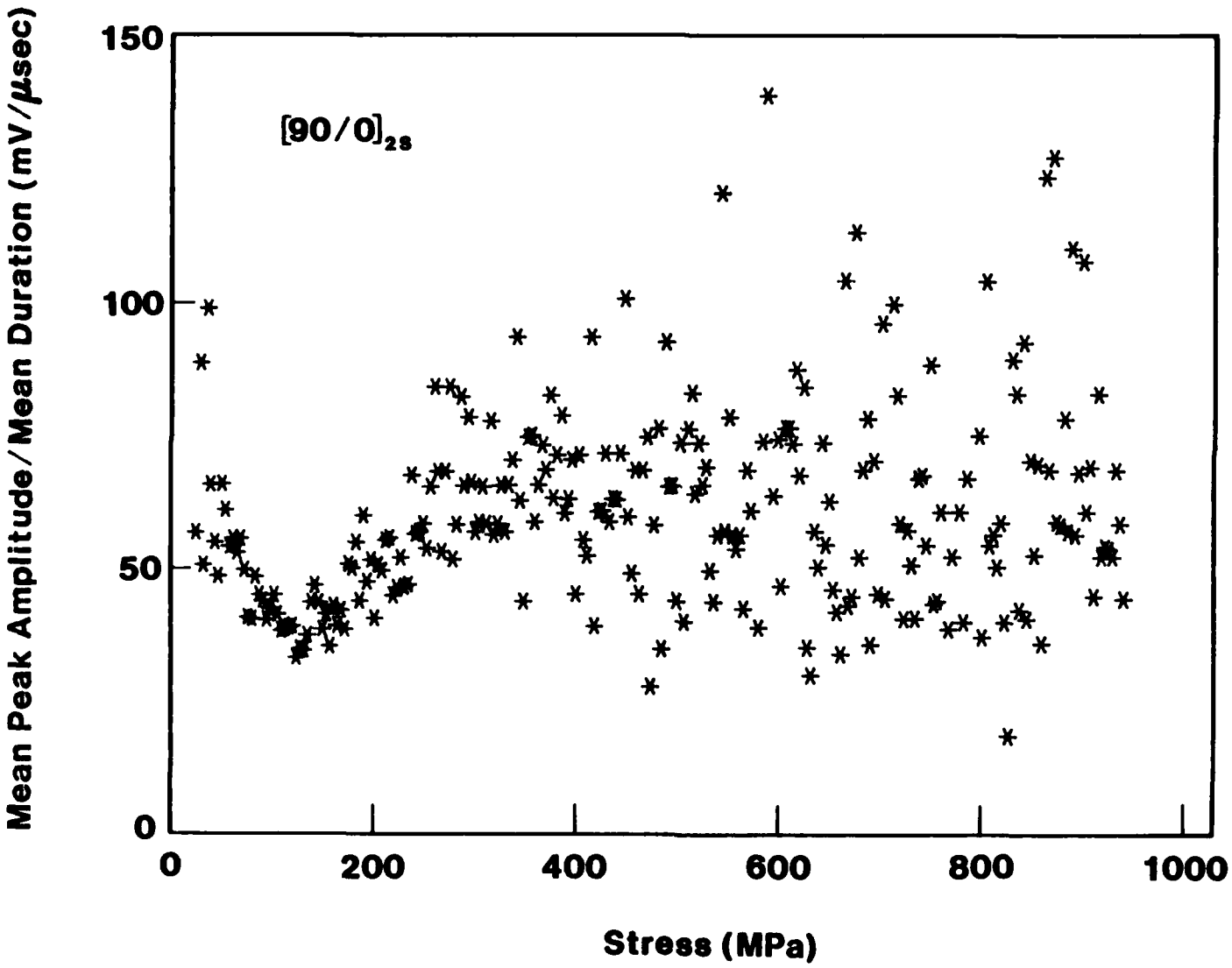

Figure 15. Ratio of Peak Amplitude to Event Duration versus Stress in $[90/0]_{2S}$ Specimen (Mean values over a 1-second interval)

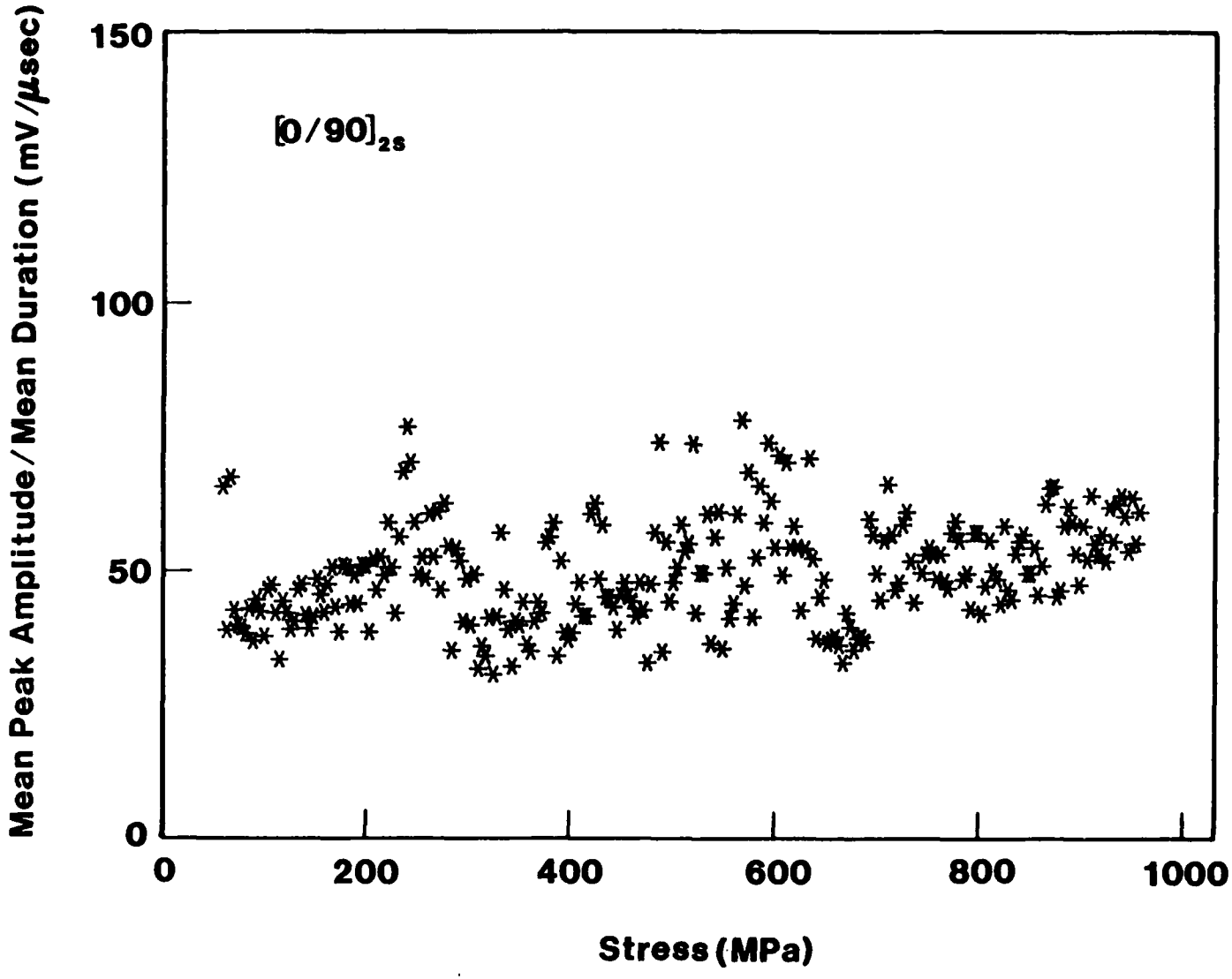

Figure 16. Ratio of Peak Amplitude to Event Duration versus Stress in $[0/90]_{2S}$ Specimen (Mean values over a 1-second interval)

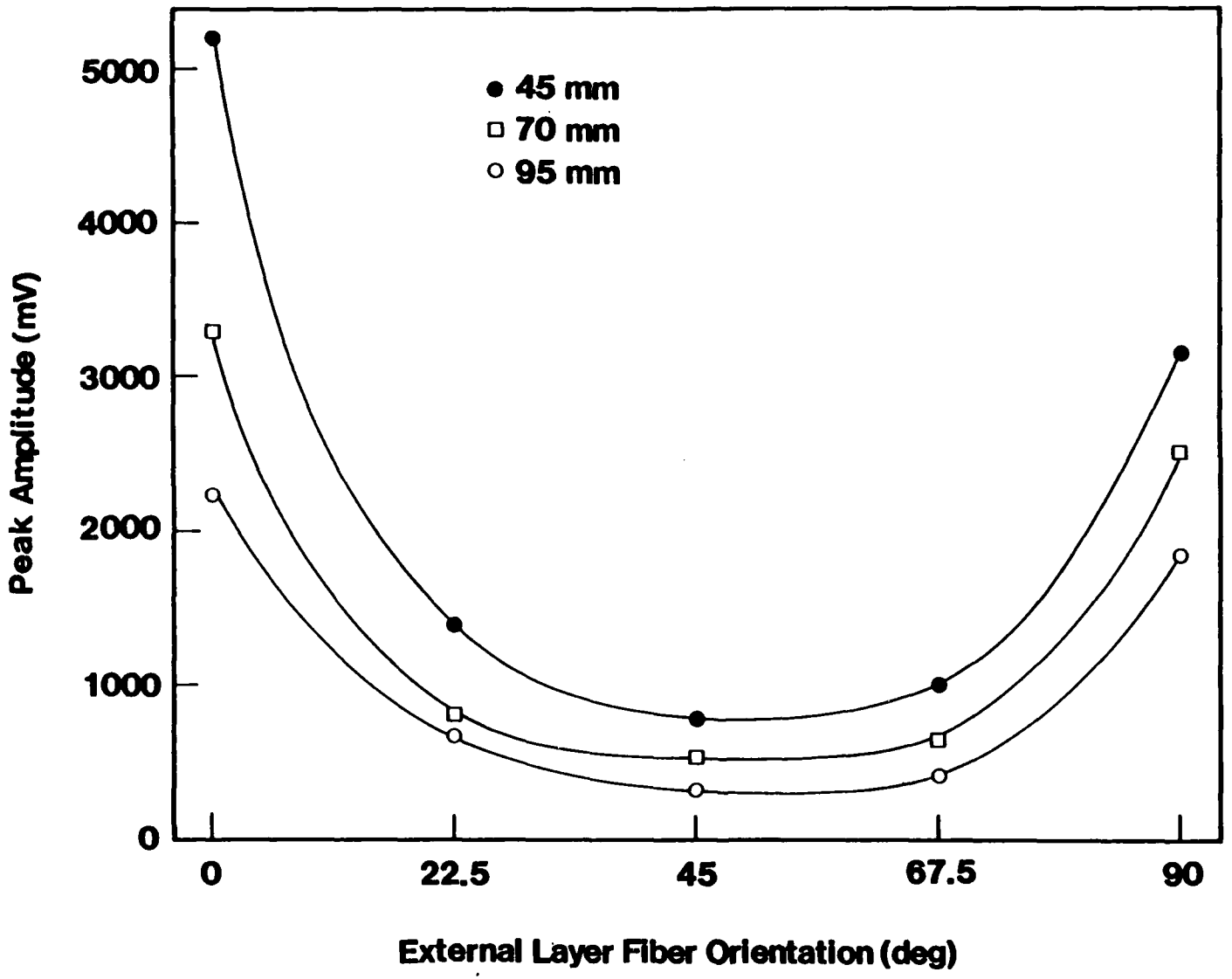

Figure 17. Variation of Peak Amplitude with Direction of Wave Propagation

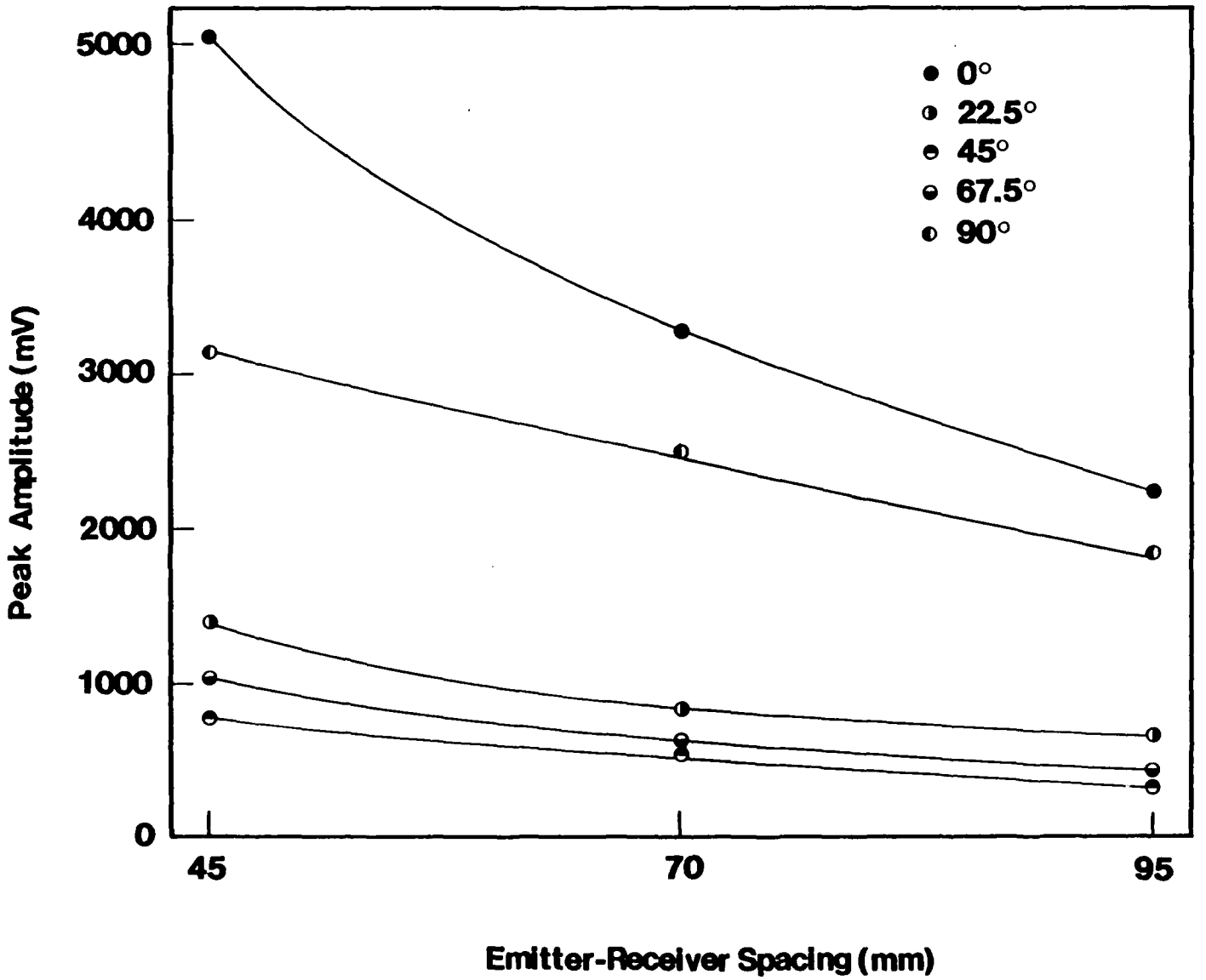

Figure 18. Variation of Peak Amplitude with Transducer Spacing

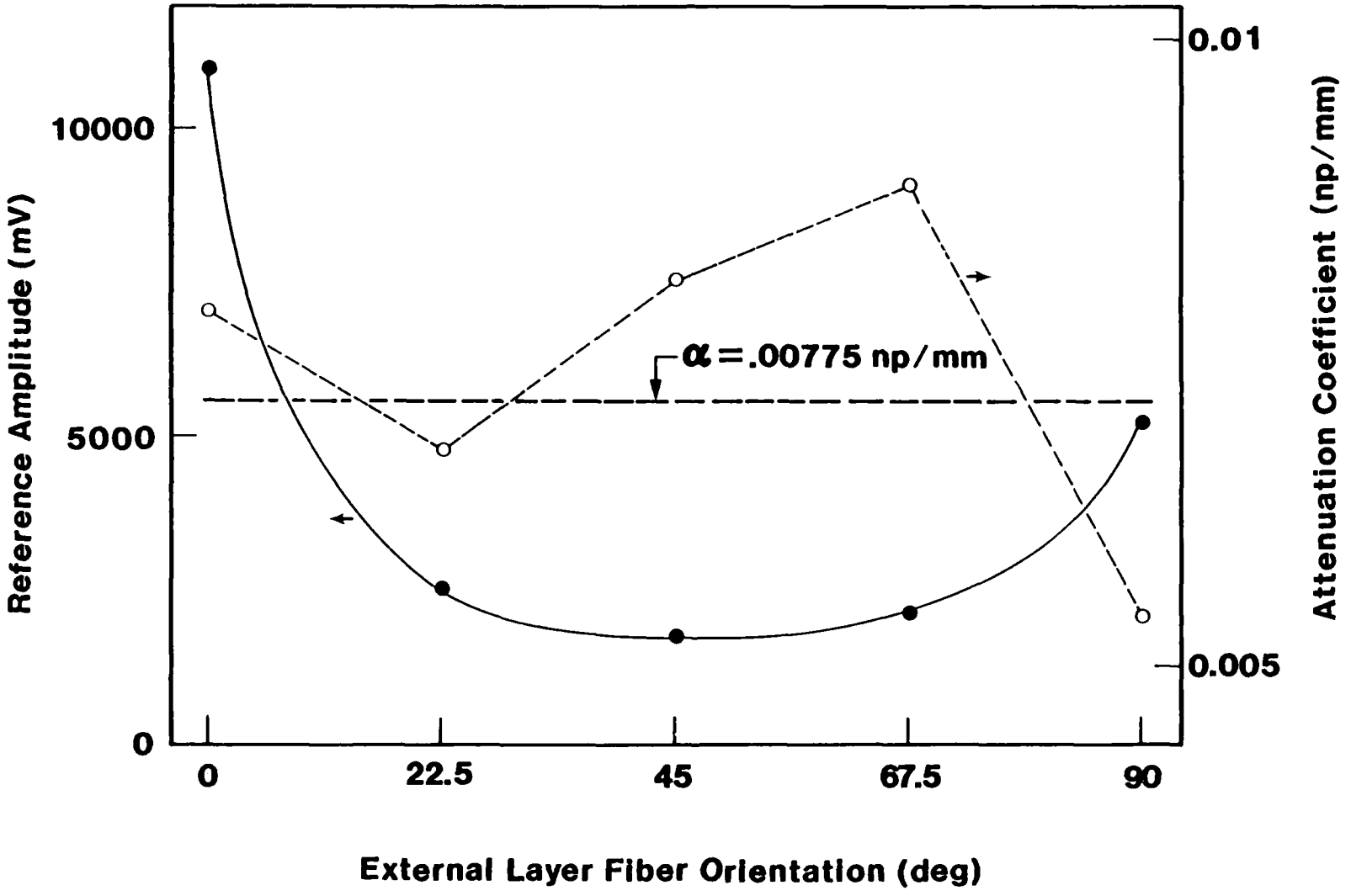

Figure 19. Dependence of Reference Amplitude and Coefficient of Apparent Attenuation on the Direction of Wave Propagation

END

DTIC

7-86